Pharmaceutical Sciences Asia

Pharm Sci Asia 2025; 52(3), 362-375
DOI:10.29090/psa.2025.03.25.5007

Research Article

Preparation, characterization, and antioxidant capacity of rosmarinic acid inclusion complexes into γ-cyclodextrin

Akiteru Ohtsu[1], Mione Uchimura[1], Nao Kodama[1], Shun-ichi Mitomo[1], Junki Tomita[2], Mitsuaki Suzuki[3], and Yutaka Inoue[1*]

[1*] Laboratory of Nutri-Pharmacotherapeutics Management, Faculty of Pharmacy and Pharmaceutical Sciences, Josai University, 1-1 Keyakidai, Sakado, Saitama 3500295, Japan
[2] Instrument Analysis Center, Josai University, 1-1 Keyakidai, Sakado, Saitama 3500295, Japan
[3] Department of Chemistry & Biological Science, Faculty of Science, Josai University, 1-1 Keyakidai, Sakado, Saitama 3500295, Japan

ABSTRACT

The purpose of this study was to prepared inclusion complexes of rosmarinic acid (RA) with γ-cyclodextrin (γ-CD) and cyclodextrin-metal–organic framework (CD-MOF) were prepared as ground mixtures (GMs) using a three-dimensional grinding method. The physicochemical properties, intermolecular interactions, solubility, and antioxidant capacity of GM (RA/γ-CD) and GM (RA/CD-MOF-1) were evaluated. Powder X-ray diffraction analysis demonstrated the disappearance of diffraction peaks in GM (γ-CD/RA = 1/1, RA/CD-MOF-1 = 1/1), suggesting that RA transformed into an amorphous state upon complexation. Differential scanning calorimetry analysis revealed that the endothermic peak of RA (~170°C), corresponding to its melting point, was absent from these complexes, indicating inclusion complex formation. Near-infrared spectroscopy exhibited peak shifts in the -CH stretching vibrations of RA, -OH groups of γ-CD, and absorption bands associated with free water, suggesting intermolecular interactions within the complexes. Dissolution tests (5 min) showed that RA had ~70% solubility, whereas the solubility of GM (RA/γ-CD) and GM (RA/CD-MOF-1) increased to ~85% and ~95%, respectively. ^{1}H-^{1}H nuclear Overhauser effect nuclear magnetic resonance spectroscopy detected cross-peaks between RA protons (H-A to H-E, H-A′ to H-C″) and γ-CD cavity protons (H-6 at 3.6 ppm, H-3 at 3.7 ppm) in GM (RA/γ-CD), confirming encapsulation. Similarly, GM (RA/CD-MOF-1) interacted with H-6 (3.65 ppm), suggesting inclusion of RA. Antioxidant assays showed marginal half-maximal inhibitory concentration improvement compared with that of RA alone (1.72 μg/mL). CD-MOF inclusion complexes show potential as platforms for improving the drug bioavailability and bioactivity in pharmaceutical formulations. These findings suggest that CD-MOF-1-based inclusion complexes could be valuable platforms for enhancing solubility and functional performance of phenolic compounds like RA in pharmaceutical applications.

Keywords:
Rosmarinic acid; Cyclodextrin; Physicochemical property; NOESY NMR spectroscopy; Antioxidant

1. INTRODUCTION

Rosmarinic acid (RA) is a phenolic acid widely found in plants, particularly in the Lamiaceae (e.g., rosemary, basil, and perilla) and Rubiaceae families. As one of the most important polyphenolic compounds, it is used in several fields, such as the food, pharmaceutical, and cosmetic industries [1]. RA is a hydroxycinnamic acid that was first isolated from the leaves of rosemary (Rosmarinus officinalis) and is abundant in other medicinal plants of the Cyperaceae family, such as spearmint and lemon balm [2]. RA is a natural polyphenolic compound

***Corresponding author:**
* Yutaka Inoue Email: yinoue@josai.ac.jp

formed by the esterification of caffeic acid and 3-(3,4-dihydroxyphenyl) lactic acid. RA exhibits various biological activities, including antiviral [3], antibacterial, anti-inflammatory, antioxidant [4], and renal protection [5]. This potent antioxidant neutralizes reactive oxygen species in the body, thereby preventing cell damage, delaying aging, and reducing the risk of chronic diseases, such as cardiovascular disease and diabetes [6,7,8,9,10]. Its antioxidant effects are particularly remarkable, and clinical trials using samples or medicinal plants with high concentrations of RA have reported favorable results. However, in vivo oral administration to rats at doses of 12.5–50.0 mg/kg shows low absolute bioavailability (0.91–1.69%) [11]. Furthermore, its solubility in acidic aqueous solution (pH 1.2) at 25°C is low at 1.8 mg/mL (5 mM) [12], limiting its application potential. Therefore, improved handling pharmaceutical formulations are required.

Metal−organic frameworks (MOFs) are porous crystalline compounds composed of metal-containing clusters that show high potential for various applications, including gas storage [13,14,15], separation technologies [16,17], sensors, and catalysis [13]. However, the toxicity of certain metals used in their synthesis restricts their applicability, posing challenges, particularly in the development and use of MOFs in pharmaceutical formulations [18]. Recently, a new edible carrier MOF, referred to as γ-cyclodextrin MOF (CD-MOF-1), has been proposed to manage this issue. CD-MOF-1 is synthesized using potassium hydroxide, ethanol, and γ-cyclodextrin (γ-CD), a cyclic oligosaccharide comprising eight glucose units linked by α-1,4-glycosidic bonds [19]. It exhibits a three-dimensional microporous structure in which potassium ions coordinate with the hydroxyl groups of eight γ-CD molecules (Fig. 1). Recent reviews have also highlighted the importance of structural design and functionalization of CD-based MOFs to optimize their performance in biomedical applications [20]. According to Patyk-Kaźmierczak et al., CD-MOF-1 exists in two polymorphic forms, α and β, depending on the absorbed water conditions, with cavity diameters of 7.8 and 4.2 Å for the α-form and β-form, respectively [21]. CD-MOF-1 has been utilized to separate various organic compounds, including saturated and unsaturated aromatic, alicyclic, chiral, and haloaromatic compounds [22]. Previous studies have evaluated the selectivity of CD-MOF-1 for incorporating compounds bearing multiple side chains, such as ascorbic acid derivatives [23]. Furthermore, inclusion complexes of CD-MOF-1 with daidzein, a soybean-derived compound, were prepared and subjected to antioxidant activity evaluation [24]. Furthermore, MOF (β-CD-CsOH) prepared using different cyclic oligosaccharides exhibited high delivery capacity for anticancer drugs such as methotrexate and 5-fluorouracil. In vitro cytotoxicity studies using HepG2 cells showed that the cytotoxicity of these drugs tended to be suppressed when bound to MOF [25]. Because CDs are derived from renewable biomass such as starch, they have also gained attention for their potential applications in sustainable resource utilization. In this context, CD-MOF-1 is postulated to function as a drug carrier with properties distinct from those of γ-CD. The ability of CD-MOF-1 to encapsulate RA, an essential oil component, is expected to open new avenues for applications in drug discovery and the food industry.

Inclusion compounds can be prepared using various methods, including coprecipitation [26], lyophilization [27], and mixed grinding [28]. CD-MOF-1, composed of γ-CD, functions as a host molecule, whereas the encapsulated molecule is referred to as a guest molecule. CDs encapsulate guest molecules to form inclusion complexes, with hydrophobic compounds included primarily through hydrophobic interactions between the guest molecules and cavity of the CD. In addition to hydrophobic interactions, dipole–dipole interactions and van der Waals forces may contribute to the binding of guest molecules. CDs can enhance the water solubility of hydrophobic molecules by incorporating appropriately sized nonpolar molecules into their cavities [29]. Similarly, inclusion complexes of rosmarinic acid with modified β-cyclodextrins have been reported to enhance solubility, physicochemical stability, and antioxidant activity [30]. Thus, the ability of γ-CD-derived CD-MOF-1 to encapsulate RA may expand the applications of RA. Recent studies have demonstrated that cyclodextrin-based carriers, including CD-MOFs, improve the solubility and antioxidant performance of RA and other polyphenols [31,32,33].

In this study, RA/γ-CD and RA/CD-MOF-1 inclusion complexes were prepared using ground mixtures of RA, γ-CD, and CD-MOF-1, and their physicochemical properties in the solid state were evaluated. The solubility of RA in the prepared complexes was assessed in distilled water and artificial intestinal fluid. The effect of CD-MOF-1 on the antioxidant activity of RA was examined using a 2,2-diphenyl-1-picrylhydrazyl (DPPH) radical-scavenging assay.

2. MATERIALS AND METHODS

2.1. Materials

RA (lot FR023101701, 023101550, and 0000028283) was purchased from Funakoshi Co. γ-CD (lot 801,005) was supplied by Cyclo Chem Bio Co., Ltd. (Tokyo, Japan)

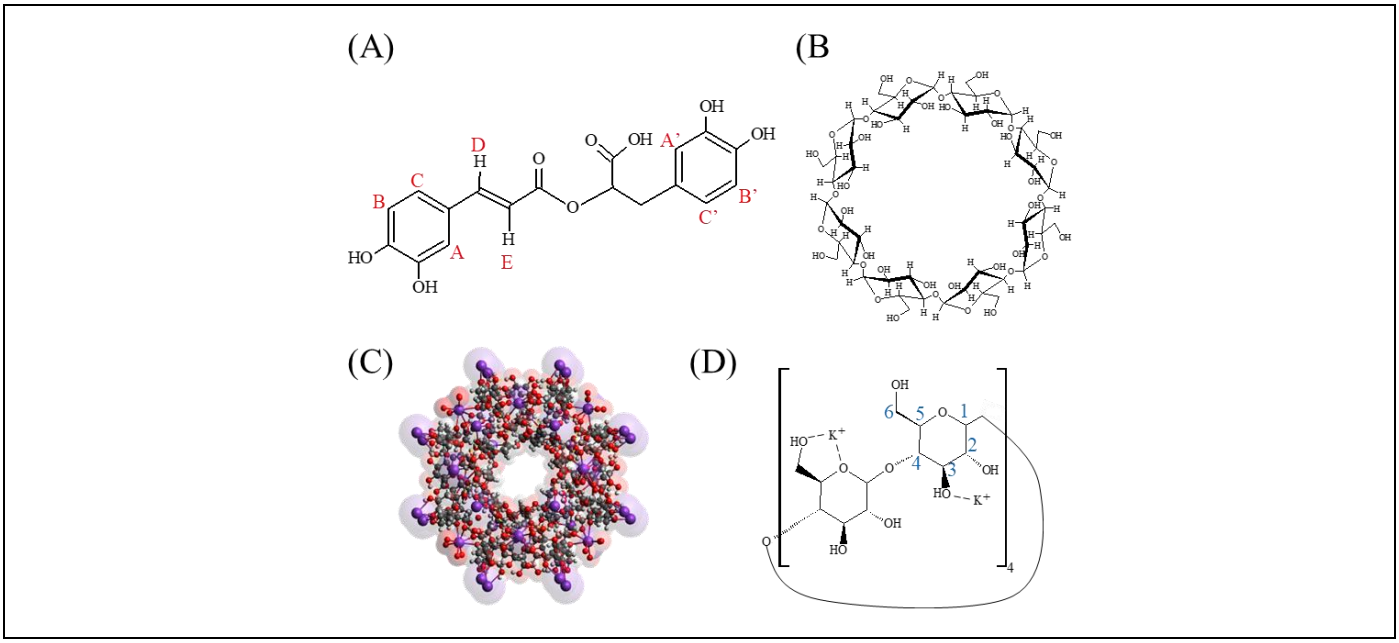

Figure 1. Chemical structure of (A) Rosmarinic Acid (RA), (B) γ-Cyclodextrin (γ-CD), (C) CD-MOF-1, (D) γ-CD(KOH)$_2$

and stored at 40°C and 82% relative humidity for 7 days (Fig. 1). DPPH (lot STBD4148) was purchased from Sigma-Aldrich (St. Louis, MO, USA). Deuterium oxide (lot C017), the nuclear magnetic resonance (NMR) solvent, was purchased from FUJIFILM Wako Pure Chemical Corporation (Osaka, Japan). Egg lecithin (lot: CAQ3804, PTL5451, and PTH4694) was purchased from FUJIFILM Wako Pure Chemical Corporation. Other reagents were of special grade and were purchased from FUJIFILM Wako Pure Chemical Corporation.

2.2. Preparation of CD-MOF-1

CD-MOF-1 was prepared as described by Smaldone, et al.[19]. γ-CD (1.0 mmol) and KOH (8.0 mmol) were dissolved in distilled water (approximately 20 mL) and vapor-diffused with ethanol (50 mL) for 1 week. The resulting crystals were filtered, washed with ethanol, and air-dried at room temperature. CD-MOF-1 was stored in a desiccator at room temperature to maintain constant moisture content. The compositional formula of one molecule of CD-MOF-1, γ-CD(KOH)$_2$, is shown in Fig. 1. γ-CD was stored at 40°C and 82% relative humidity for 7 days to ensure consistent hydration, which affects its crystalline form and potential for inclusion complex formation. CD-MOF-1 was used as prepared without additional conditioning.

2.3. Preparation of physical mixture (PM) and ground mixture (GM)

The physical mixtures (PMs) were prepared by weighing RA and γ-CD or CD-MOF-1 in an equimolar ratio (1:1) and mixing them in a vortex mixer for 1 min. Subsequently, 500 mg of each PM (RA/γ-CD or RA/CD-MOF-1) was transferred into a 100 g milling jar along with 5 mm-diameter stainless steel milling balls. The mixtures were then subjected to grinding for 30 min using a three-dimensional (3D) ball mill (3D-80, Nagao System Inc., Yokohama, Japan). The resulting products were designated as ground mixtures (GMs). The grinding process was designed to induce mechanochemical interactions between RA and the host materials, thereby promoting the formation of inclusion complexes. The grinding time (30 min) was selected based on our previous reports and preliminary experiments, in which inclusion complexes with compounds such as daidzein and FAD012 were successfully formed using γ-CD or CD-MOF-1 under similar 3D ball-milling conditions [24,34]. An equimolar ratio (1:1) of RA to CD was chosen to ensure efficient complexation and to allow consistent comparison between γ-CD and CD-MOF-1 systems.

2.4. Fasted-state simulated intestinal fluid (FaSSIF)

FaSSIF was prepared as follows. Sodium dihydrogen phosphate dihydrate and sodium chloride were dissolved in distilled water to concentrations of 31.526 and 116.6 mM, respectively [35]. Subsequently, the pH was adjusted to pH 6.5 with sodium hydroxide solution, and 100 mL of stock solution was prepared. To prepare 500 mL of FaSSIF solution, sodium taurocholate (NaTC) was used to prepare a NaTC solution (12 mM) using 125 mL of the prepared stock solution and a final FaSSIF concentration of 3 mM. In addition, 0.2856 g of lecithin was weighed to obtain a final FaSSIF concentration of 0.75 mM and dissolved in 3 mL of dichloromethane in an eggplant flask. Next, 125 mL of NaTC solution was added to the lecithin

solution using sonication, followed by decompression in a rotary evaporator at 40°C and 350 mbar for 15 min to remove the dichloromethane. If the cloudy solution became clear but the odor of dichloromethane was still felt, the pressure was further reduced to 250 mbar for 5 min. To the solution prepared under reduced pressure, 325 mL of the stock solution was added, and distilled water was added to prepare 500 mL of FaSSIF solution.

2.5. Powder X-ray diffraction measurement (PXRD)

PXRD was performed using a MiniFlex II powder X-ray diffractometer (Rigaku Corporation, Tokyo, Japan). The measurement conditions were as follows: an NaI scintillation counter was used to measure the diffraction intensity, irradiation dose was Cu wire (30 kV, 15 mA), scan speed was 3.00°/min, and measurement range was $2\theta = 5–35°$. The powder sample was held on a glass plate and the sample surface was filled flat for measurement.

2.6. Differential scanning calorimetry (DSC)

DSC was performed using a ThermoPlus Evo high-sensitivity differential scanning calorimeter (Rigaku Corporation). Measurements were performed with approximately 3 mg of sample in a sealed aluminum pan under nitrogen gas flow (60 mL/min) while increasing the temperature at a rate of 5°C/min from 30°C to 360°C.

2.7. Infrared absorption spectrum measurement

Fourier-transform infrared (FT-IR) spectra were measured using the KBr plate method on a JASCO FT/IR-4600 (JASCO Corporation, Tokyo, Japan) in the range of 4000–400 cm^{-1} for 16 integration cycles at 4 cm^{-1} resolution.

2.8. Near-infrared (NIR) absorption spectrum measurement

NIR absorption spectra were obtained using a Fourier-transform NIR spectrometer (JASCO V-770). The conditions were as follows: measurement wavenumbers of 10,000–4000 cm^{-1}, measurement time of 8 s, and measurement temperature of 25°C. Each sample was filled into a sample cup and measurements were performed at intervals of 2 nm in the optical path.

2.9. Scanning electron microscope measurements

Scanning electron microscopy (SEM) was performed using a JSM-IT800 (SHL) microscope (JEOL, Tokyo, Japan) at an acceleration voltage of 1 kV. The samples were then gold-coated under vacuum for 60 s.

2.10. Dissolution test

The dissolution test was performed using an NTR-593 dissolution tester (Toyama Sangyo Co., Ltd., Osaka, Japan) according to the paddle method of the Japanese Pharmacopoeia, 18th edition. The paddle speed was 50 rpm and the test solution was distilled water and FaSSIF (300 mL each, 37°C ± 0.5°C), and quantification was performed using high-performance liquid chromatography. RA was detected using a Waters e2695 UV-visible photometer (Milford, MA, USA) at 330 nm. The column was COSMOSIL (4.6 ID × 150 mm, Φ5 μm, lot K51712; Nacalai Tesque, Kyoto, Japan), sample injection volume was 50 μL, column temperature was 40°C, mobile phase was KH_2PO_4 (10 mM, pH2.0)/CH_3CN (50/50), and retention time was 6 min. An amount of the inclusion complex equivalent to 30 mg of RA was added to the paddle apparatus. Each dissolved sample of 5 mL was collected at 5, 10, 15, 30, 60, and 120 min and filtered through a 0.20-μm polytetrafluoroethylene membrane filter (DISMIC®-25AS, ADVANTEC®, Toyo Roshi Company, Ltd, Tokyo, Japan). The total volume of the solution was maintained constant throughout the experiment. To maintain the total solution volume throughout the experiment, the same temperature and volume of solution were added after each sample collection.

2.11. ^1H-^1H nuclear Overhauser effect NMR spectroscopy

An NMR system operating at 700 MHz (Agilent Technologies, Santa Clara, CA, USA) was used. The solvent was deuterium oxide, resonance frequency was 699.6 MHz, pulse width was 10.05°, and relaxation time was 1.000 s at 20°C [36].

2.12. DPPH radical-scavenging test

DPPH/CH_2CN solution (100 μM) and each sample solution were mixed in a microplate in a 1/1 ratio and incubated at 37°C for 30 min under light-shielded conditions; the absorbance of DPPH was measured at 517 nm. Absorbance was measured using a Spectra Max M2e (Molecular Devices, Sunnyvale, CA, USA). The mixture of distilled water/ (DPPH/CH_2CN solution) (1/1) was used as 0% radical removal (A_0) and the mixture of distilled water/CH_2CN (1/1) as 100% radical removal (Blank: Bl). The DPPH radical-scavenging activity was calculated using Equation (1).

$$\text{Radical-scavenging rate} = [1-(\text{absorbance} - \text{Bl})/ (A_0 - \text{Bl})] \times 100 \quad (1)$$

2.13. Statistical analysis

Data are expressed as the mean ± standard deviation. Comparisons between experimental groups were assessed using the Tukey's test and one-way analysis of variance multiple comparison test (with $p < 0.01$ and $p < 0.05$ indicating significant differences) using Statcel—the Useful Addin Forms on Excel, 4th ed.

3. RESULTS AND DISCUSSION

3.1. PXRD

PXRD measurements were performed to investigate the changes in the crystalline form in the GM of RA/γ-CD and RA/γ-CD-MOF-1 (Fig. 2). Characteristic diffraction peaks of intact RA were observed at 2θ = 13.6°, 14.9°, 19.6°, and 26.6° (Fig. 2(a)). γ-CD exhibited characteristic diffraction peaks at 2θ = 9.8° and 12.0° (Fig. 2(b)), whereas CD-MOF-1 showed a characteristic diffraction peak at 2θ = 7.0° (Fig. 2(c)). PM (RA/γ-CD = 1/1) and PM (RA/CD-MOF-1 = 1/1) exhibited characteristic diffraction peaks derived from RA, γ-CD, and CD-MOF-1, respectively (Fig. 2(d), (f)). In contrast, GM (RA/γ-CD = 1/1) and GM (RA/CD-MOF-1 = 1/1) showed halo patterns, accompanied by the disappearance of diffraction peaks derived from RA, γ-CD, and CD-MOF-1 (Fig. 2(e), (f)). When CDs encapsulate drug molecules to form inclusion complexes, their intermolecular interactions and molecular arrangements change, leading to the collapse of the original crystal structure. To further clarify the role of cyclodextrins in the amorphization of RA, a supplementary PXRD analysis was conducted for RA before and after grinding alone for 30 minutes. As shown in Figure 1S, the diffraction peaks of RA remained after grinding, indicating that RA did not convert to an amorphous state by mechanical grinding alone. In contrast, co-grinding with γ-CD or CD-MOF-1 led to the disappearance of these peaks and the appearance of a halo pattern. This supports the conclusion that amorphization occurred as a result of inclusion complex formation with the host molecules, and not merely due to mechanical force. Consequently, the crystallinity decreased and an amorphous-like structure was generated. In inclusion complexes, drug molecules are accommodated within the cavity of CDs, causing molecular disorder that often results in decreased diffraction peak intensity or peak broadening, leading to the observation of a halo pattern [37]. Based on these results, the disappearance of characteristic diffraction peaks derived from RA crystals in GM (RA/γ-CD = 1/1) and GM (RA/CD-MOF-1 = 1/1) suggests that mechanochemical grinding induced a change in the crystalline state, promoting complex formation.

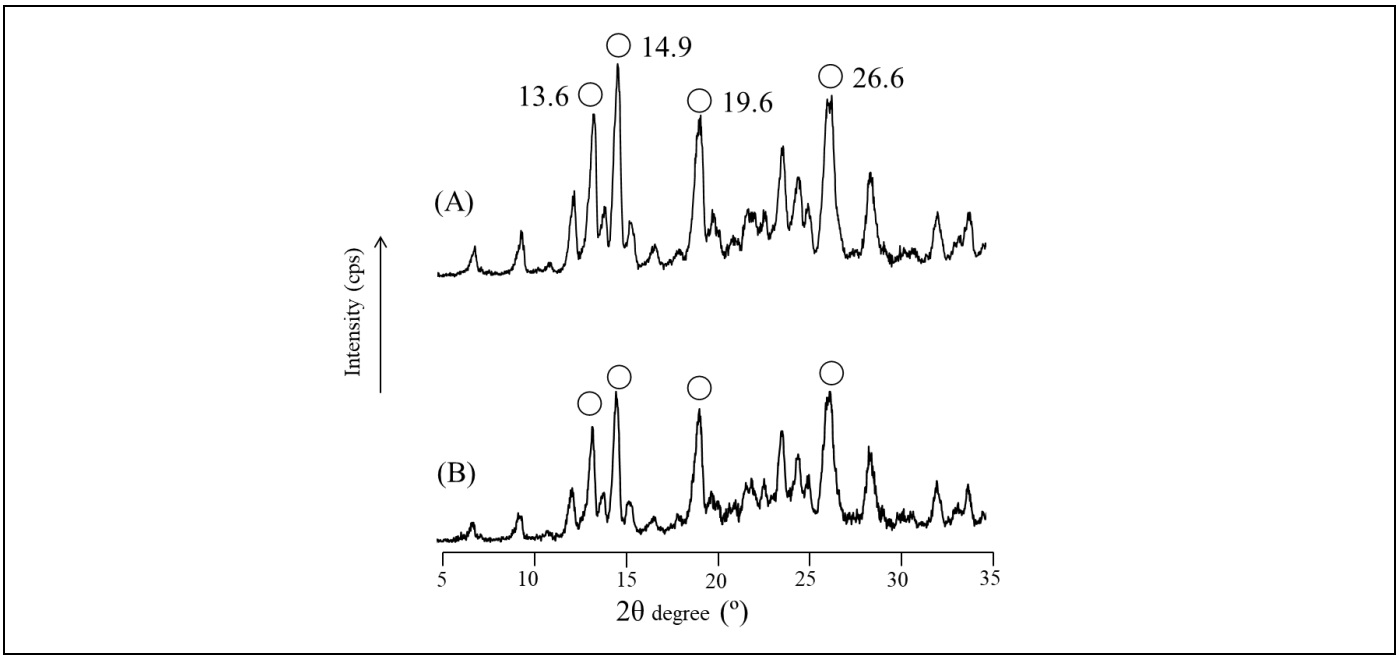

Figure 1S. Powder X-ray diffraction patterns of (A) intact rosmarinic acid (RA) and (B) RA after 30 minutes of mechanical grinding without any cyclodextrin. The diffraction peaks remained, indicating that RA did not become amorphous by grinding alone.

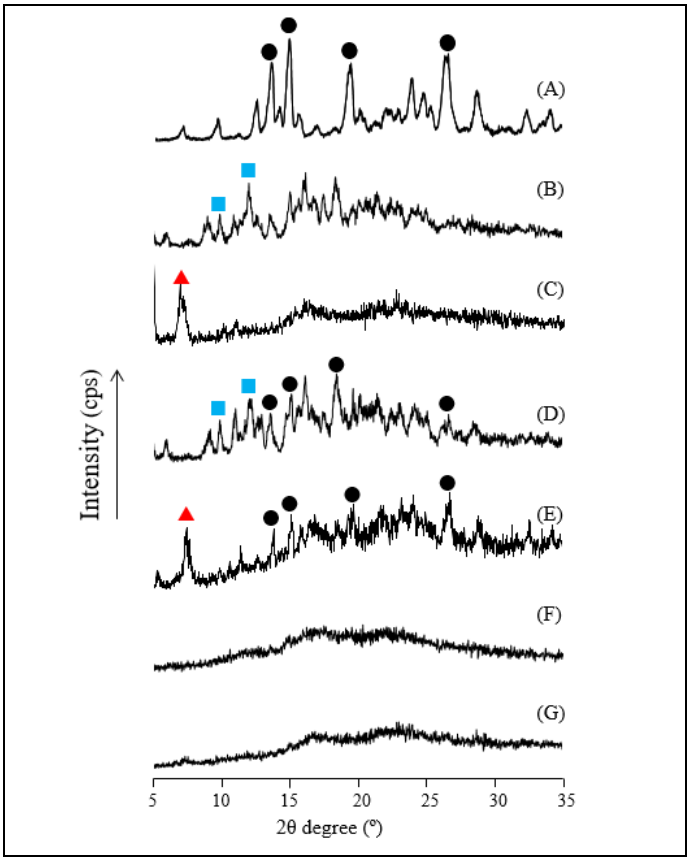

Figure 2. PXRD patterns of RA intact, RA/γ-CD, RA/CD-MOF-1 systems. (A) RA, (B) γ-CD, (C) CD-MOF-1, (D) PM(RA/γ-CD=1/1), (E) PM(RA/CD-MOF-1=1/1), (F) GM(RA/γ-CD=1/1), (G) GM(RA/CD-MOF-1=1/1)

3.2. DSC

The results of PXRD analysis suggest that inclusion complexes were formed in both GM (RA/γ-CD = 1/1) and GM (RA/CD-MOF-1 = 1/1). The formation of inclusion complexes has been reported to alter the thermal behavior of guest molecules, such as through the disappearance or shift in their melting points. Therefore, DSC measurements were conducted to investigate the thermal behavior resulting from complex formation between RA and CD-MOF-1 (Fig. 3). Intact RA exhibited an endothermic peak at approximately 170°C, corresponding to its melting point (Fig. 3(a)). γ-CD showed a dehydration peak owing to the adsorbed water at approximately 113°C and a decomposition peak at around 286°C (Fig. 3(b)). CD-MOF-1 showed a dehydration peak at approximately 87°C and a decomposition peak at around 241°C (Fig. 3(c)). PM (RA/γ-CD = 1/1) exhibited an endothermic peak at approximately 170°C, corresponding to the melting of RA, indicating the presence of RA in its crystalline form (Fig. 3(d)). PM (RA/CD-MOF-1 = 1/1) showed a shift in the RA melting peak to a lower temperature, around 154°C, but the peak was still present, suggesting a partial interaction between RA and CD-MOF-1 while maintaining the presence of RA crystals (Fig. 3(e). In contrast, for GM (RA/γ-CD = 1/1), the RA melting peak disappeared, and the γ-CD decomposition peak shifted to approximately 250°C (Fig. 3(f)). Similarly, for GM (RA/CD-MOF-1 = 1/1), the RA melting peak disappeared, and the CD-MOF-1 decomposition peak shifted to around 262°C (Fig. 3(g)). A previous study of the formation of inclusion complexes between β-CD and naproxen showed that complete encapsulation of crystalline drugs inside the CD cavity is often evidenced by disappearance of the drug's melting peak in DSC thermograms [38]. When an inclusion complex is formed, the drug molecules are encapsulated within the CD cavity, preventing them from maintaining their crystalline state and leading to collapse of their crystal structure. During the formation of inclusion complexes between CDs and drugs, intermolecular interactions such as hydrophobic interactions, dipole interactions, and van der Waals forces restrict the mobility of drug molecules and alter the energy state required for melting. Consequently, the endothermic peak corresponding to the melting point disappears [39]. According to these results, the formation of inclusion complexes in GM (RA/γ-CD = 1/1) and GM (RA/CD-MOF-1 = 1/1) may have altered the thermal behavior of RA by encapsulating it within the cavities of γ-CD and CD-MOF-1, resulting in disappearance of the melting

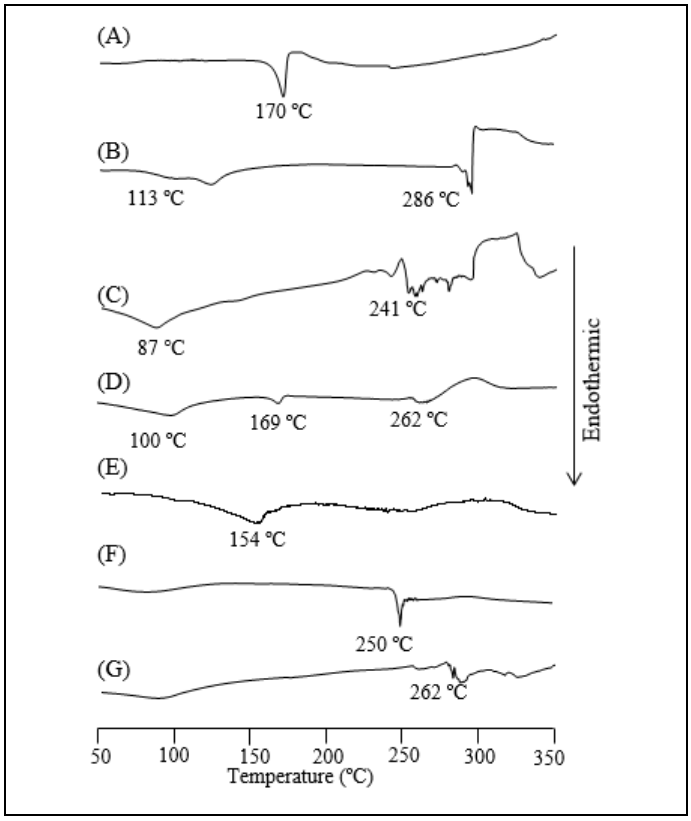

Figure 3. DSC curves of RA, RA/γ-CD, RA/CD-MOF-1 systems. (A) RA, (B) γCD, (C) CD-MOF-1, (D) PM(RA/γCD=1/1), (E) PM(RA/CD-MOF-1=1/1), (F) GM(RA/γCD=1/1), (G) GM(RA/CD-MOF-1=1/1)

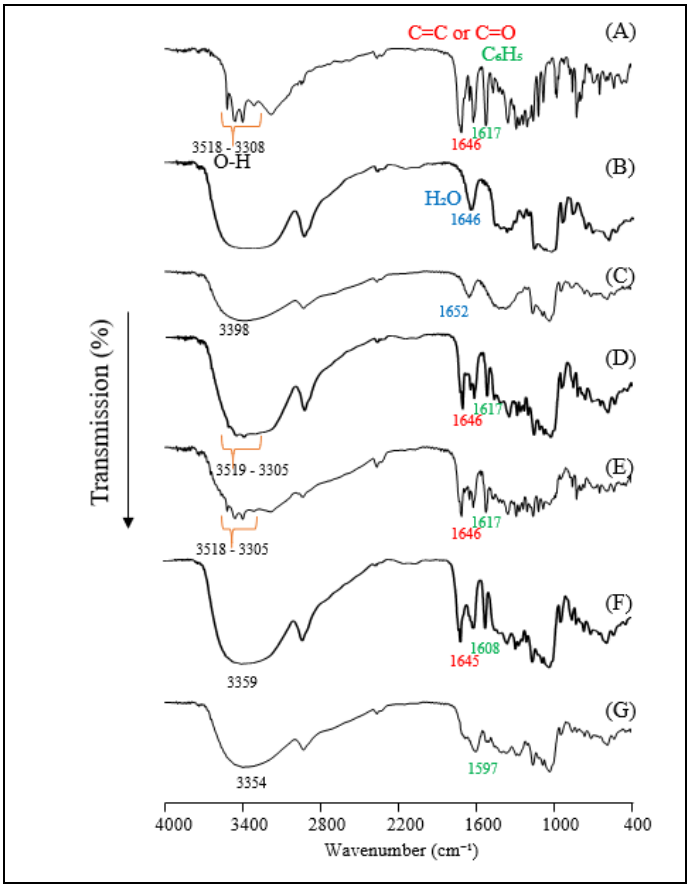

Figure 4. FT-IR spectra of RA intact, RA/γ-CD, RA/CD-MOF-1 systems. (A) RA, (B) γCD, (C) CD-MOF-1, (D) PM(RA/γCD=1/1), (E) PM(RA/CD-MOF-1=1/1), (F) GM(RA/γCD=1/1), (G) GM(RA/CD-MOF-1=1/1)

peaks. These observations suggest that the crystalline structure of RA disappeared and that amorphous or complexed forms were formed in the GM samples.

3.3. FT-IR spectroscopy

The PXRD and DSC results indicated that inclusion complexes formed in GM (RA/γ-CD = 1/1) and GM(RA/CD-MOF-1 = 1/1). FT-IR spectroscopy is a useful technique for identifying intramolecular and intermolecular interactions between drugs. Particularly, when hydrogen bonding contributes to intermolecular interactions between drugs or among drugs and excipients, peak shifts in functional groups such as hydroxyl and carbonyl groups occur [34]. Therefore, FT-IR measurements were conducted to investigate the intermolecular interactions between RA, γ-CD, and CD-MOF-1 (Fig. 4). In intact RA, a peak derived from the aromatic ring of RA was observed at 1608 cm^{-1}, a peak derived from the vinyl or carbonyl group appeared at 1646 cm^{-1}, and a peak corresponding to the hydroxyl group was observed at 3308–3518 cm^{-1} (Fig. 4(a)). In γ-CD, a hydroxyl group-derived peak was detected at 3340 cm^{-1} (Fig. 4(b)). In CD-MOF-1, a hydroxyl group peak was observed at 3398 cm^{-1}, along with a peak at 1652 cm^{-1} corresponding to water molecules encapsulated within the structure (Fig. 4(c)). In PM (RA/γ-CD = 1/1) and PM (RA/CD-MOF-1 = 1/1), peaks derived from the aromatic ring, vinyl or carbonyl group, and hydroxyl group of RA were observed (Fig. 4(d), (e)). In contrast, in GM (RA/γ-CD = 1/1), the aromatic ring-derived peak of RA shifted to a lower wavenumber at 1607 cm^{-1}, and the peak corresponding to the vinyl or carbonyl group disappeared (Fig. 4(f)). In GM (RA/CD-MOF-1 = 1/1), the aromatic ring-derived peak of RA shifted further to 1597 cm^{-1}, and the vinyl or carbonyl group-derived peak disappeared. Additionally, the hydroxyl group-derived peak of CD-MOF-1 shifted to a lower wavenumber at 3354 cm^{-1}, and the peak corresponding to encapsulated water molecules broadened (Fig. 4(g)). These findings suggest that the hydroxyl, vinyl, or carbonyl groups of RA form intermolecular interactions with γ-CD and CD-MOF-1 through inclusion within their cavities, leading to the formation of inclusion complexes in the solid state [40,41].

3.4. NIR spectroscopy measurements

The FT-IR measurements of GM (RA/γ-CD = 1/1) and GM (RA/CD-MOF-1 = 1/1) indicated solid-state molecular interactions between the hydroxyl groups of γ-CD and CD-MOF-1 and the vinyl or carbonyl groups of RA. However, FT-IR spectroscopy has a limited ability to precisely assign the interactions between hydroxyl and alkyl groups. Therefore, NIR spectroscopy was performed to focus on these functional groups and further investigate their detailed molecular interactions (Fig. 5). In RA, peaks corresponding to -CH groups from the aromatic ring (benzene ring) were observed at 4428 and 8992 cm^{-1}, whereas peaks from alkyl groups appeared at 4306 and 8591 cm^{-1} (Fig. 5A, B-(a,c)). The hydroxyl group peaks of γ-CD were detected at 4995 and 7163 cm^{-1} (Fig. 5A-(a,b)). In PM (RA/γ-CD), the -CH peak at 4428 cm^{-1}, derived from the benzene ring of RA, overlapped with the γ-CD-derived peak, resulting in a shoulder peak that was difficult to distinguish. However, the peak at 8992 cm^{-1} remained observable, and alkyl group-derived peaks were detected at 4306 and 8591 cm^{-1}. In contrast, GM (RA/γ-CD) exhibited a shift of the benzene ring-derived -CH peak to 4464 cm^{-1}, along with a broad peak at around 8960 cm^{-1}. Additionally, the alkyl group-derived peaks of RA shifted to 4306 cm^{-1} and showed broadening around 8560 cm^{-1}. The hydroxyl group peaks of γ-CD also shifted to 4975 and 7112 cm^{-1}. Peak broadening and shifting in the NIR spectra indicated intermolecular interactions involving the corresponding functional groups [37]. For CD-MOF-1, peaks corresponding to hydroxyl groups from glucose units were observed at 5086 and 7183 cm^{-1} (Fig. 5B-(a,c)). In PM (RA/CD-MOF-1 = 1/1), broad peaks appeared

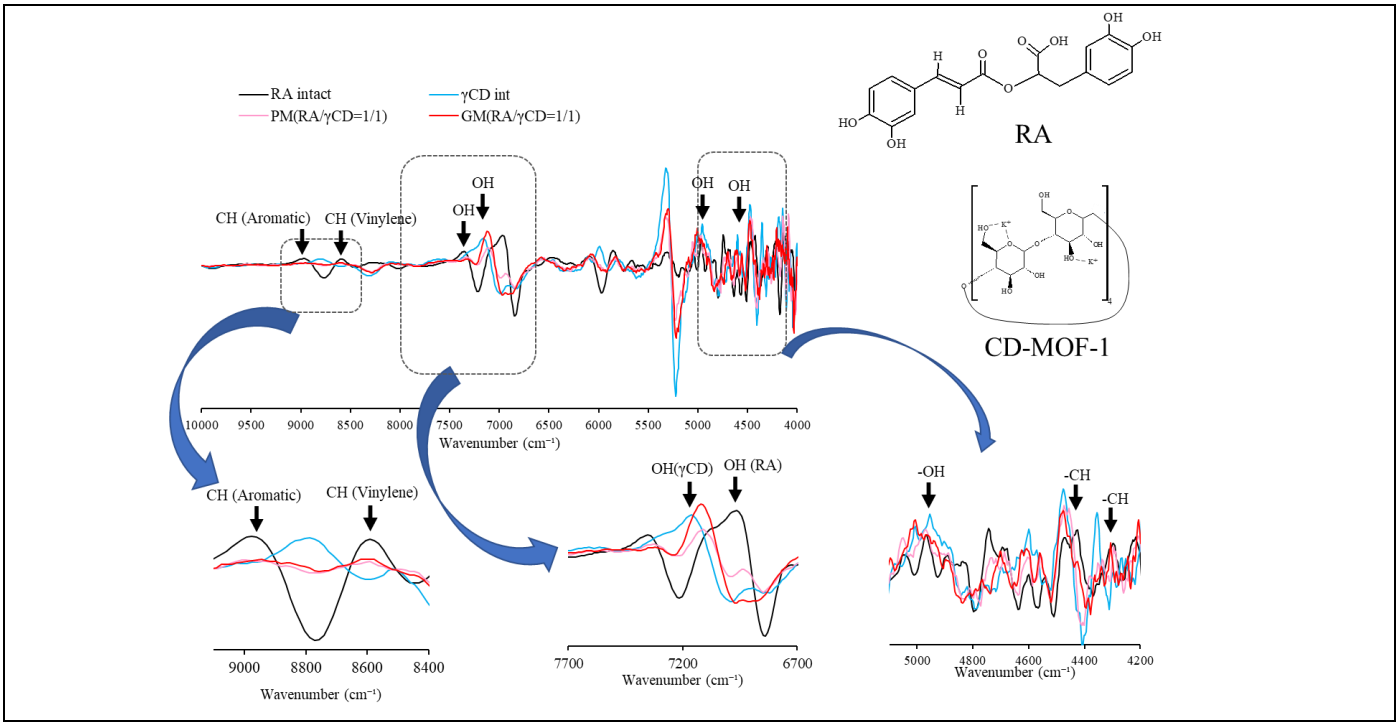

Figure 5A. Second differentiation NIR absorption spectra of RA/γCD systems: (a) 9100-8400 cm^{-1}, (b) 7700-6700 cm^{-1}, (c) 5100-4600 cm^{-1}

around 4428 and 8970 cm^{-1} for the aromatic ring and alkyl groups of RA, whereas alkyl group-derived peaks were observed at 4284 and 8576 cm^{-1} (Fig. 5B-(a,c)). In GM (RA/CD-MOF-1 = 1/1), peak shifts of the aromatic ring and alkyl groups of RA were detected at 4436 and 8912 cm^{-1}, respectively (Fig. 5B-(a,c)). Additionally, the alkyl group peak of RA shifted to 4306 cm^{-1}, with broadening around 8547 cm^{-1}. The hydroxyl group peaks derived from CD-MOF-1 also shifted to 5055 and 7112 cm^{-1} (Fig. 5C-(c-3), (b-3)). Peak broadening and shifting in the NIR spectra suggest intermolecular interactions involving the corresponding functional groups [42,43].

The results of solid-state analysis of GM (RA/γ-CD) and GM (RA/CD-MOF-1) suggest the formation of inclusion complexes through intermolecular hydrogen bonding interactions between the hydroxyl and alkyl groups of RA and the hydroxyl groups of CD-MOF-1 within the CD cavities.

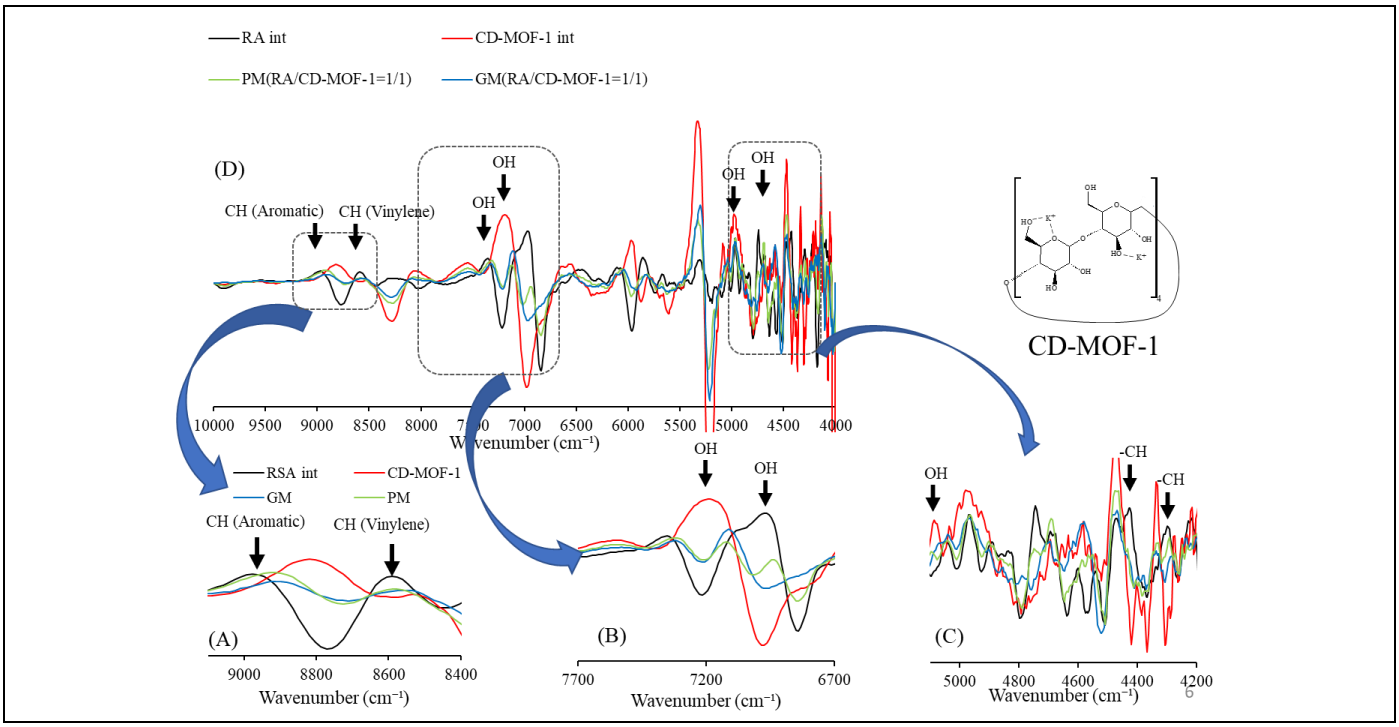

Figure 5B. Second differentiation NIR absorption spectra of RA/CD-MOF-1 systems: (a) 9100-8400 cm^{-1}, (b) 7700-6700 cm^{-1}, (c) 5100-4600 cm^{-1}

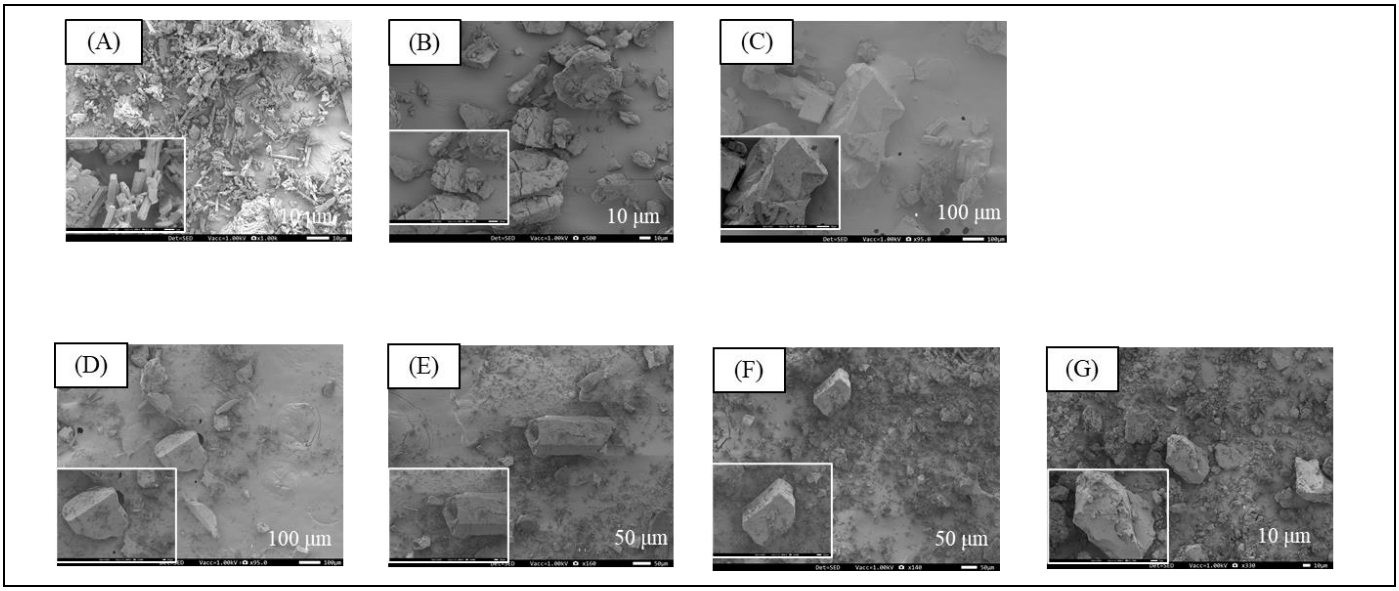

Figure 6. SEM morphology of RA/γ-CD and RA/CD-MOF-1 systems.
(A) RA (x1000), (B) γ-CD (x500), (C) CD-MOF-1 (x95), (D) PM(RA/γ-CD=1/1) (x95), (E) PM(RA/CD-MOF-1=1/1) (x160), (F) GM(RA/γ-CD=1/1) (x140), (G) GM(RA/CD-MOF-1=1/1) (x330).

3.5. SEM

The results of PXRD, DSC, FT-IR, and NIR measurements suggested the formation of a complex in GM (RA/CD-MOF-1 = 1/1). Furthermore, the PXRD results indicated changes in the crystalline state. SEM is a useful technique for analyzing the morphology of drug particles. Therefore, SEM was used to observe the morphology and surface characteristics of the RA/CD-MOF-1 complexes (Fig. 6). RA exhibited a smooth surface with prismatic crystalline particles (Fig. 6(a)). γ-CD showed a smooth surface with hexagonal and polyhedral crystalline structures (Fig. 6(b)). CD-MOF-1 displayed a smooth surface with cubic crystalline particles (Fig. 6(c)). In PM (RA/γ-CD = 1/1) and PM (RA/CD-MOF-1 = 1/1), no significant changes were observed in the particle surfaces (Fig. 6(d), (f)). In contrast, in GM (RA/γ-CD = 1/1) and GM (RA/CD-MOF-1 = 1/1), RA aggregated around the CD-MOF-1 crystals (Fig. 6(e), (g)). γ-CD-based inclusion complexes formed with CD-MOF-1 typically exhibit a cubic morphology [44]. In the present study, cubic particles were also observed in GM (RA/CD-MOF-1 = 1/1), suggesting that RA and CD-MOF-1 formed inclusion complexes in the solid state.

3.6. Dissolution tests (distilled water and FaSSIF)

DSC, PXRD, and NIR results suggested the feasibility of GM (RA/γ-CD) and GM (RA/CD-MOF-1)) inclusion complex formation. RA alone, PM (RA/γ-CD), GM (RA/γ-CD), PM (RA/γ-CD), GM (RA/CD-MOF-1)

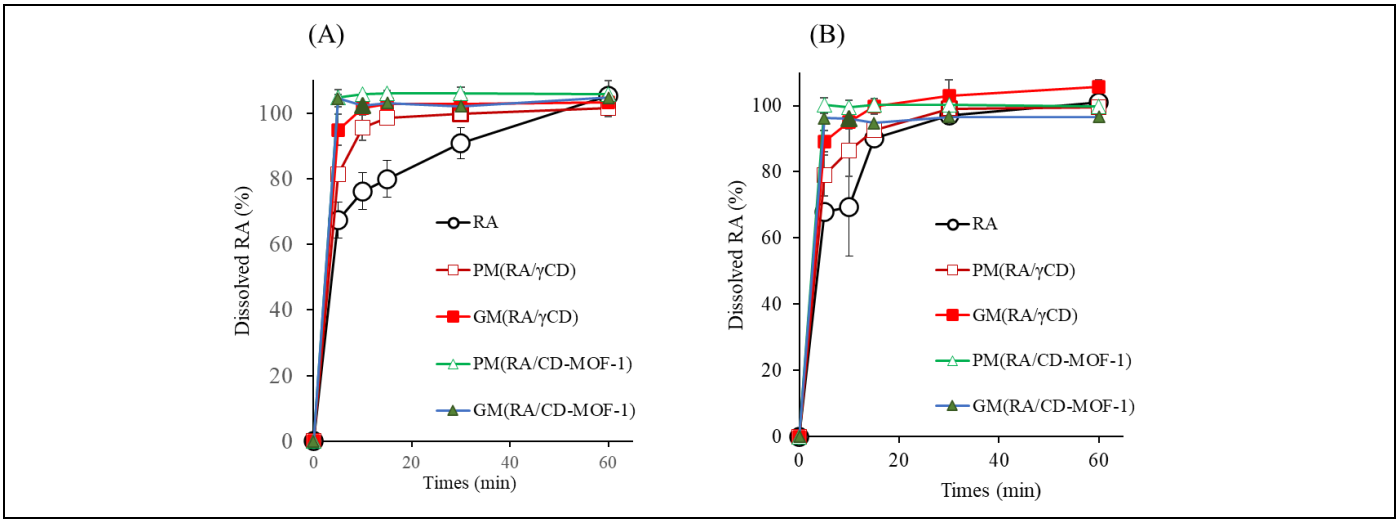

Figure 7. Dissolution profiles of RA/γ-CD and RA/CD-MOF-1 systems. (A) Distilled water, (B) FaSSIF Results were expressed as mean ± SD (n = 3).

samples were used to check the elution rate of RA into distilled water (Fig. 7(A)). RA showed an approximate dissolution rate of 70% at 5 min after its start of the RA. For PM (RA/γ-CD), this rate was approximately 77%, whereas for GM(RA/γ-CD), it was 90%. In contrast, the dissolution rates of PM (RA/CD-MOF-1) and GM (RA/CD-MOF-1) were approximately 97%, indicating rapid dissolution immediately after starting the analysis [19]. A possible reason for the improved elution of GM compared to that of RA is complex formation in the solid state, as well as from the results of the SEM measurements, which could be due to finer granulation in the grinding process. Additionally, the inclusion complex in the GM contributed to the improved dissolution rate of RA. However, PM (RA/CD-MOF-1) and GM (RA/CD-MOF-1) showed improved solubility compared to that of RA alone after 5 min. This may be because hydrogen bonding and hydrophobic interactions between CD and guest molecules contribute to the improved solubility and that γ-CD itself is water-soluble and the MOF structure further interacts with the solvent [45]. In addition, CD-MOFs have a larger specific surface area than conventional CD inclusion complexes, which increases their exposure to solvents and contributes to improved solubility [46]. The structural design and functional modification of CD-based MOFs have been increasingly recognized in recent reviews as key strategies for optimizing their functionality in biomedical applications [20]. The inclusion of RA into the cavities of CD-MOF-1 and γ-CD may improve their solubility. However, our results showed that PM (RA/CD-MOF-1) and GM (RA/CD-MOF-1) exhibited enhanced dissolution. The enhanced solubility of rosmarinic acid (RA) is likely due to acid–base interactions, given that RA is an acidic compound and CD-MOF-1 is a basic framework containing potassium. The presence of CD-MOF-1 in distilled water appears to facilitate RA solubilization through this mechanism. A dissolution study using artificial intestinal fluid was conducted to verify these possibilities. To evaluate the solubility and absorption of drugs under physiological gastrointestinal conditions, FaSSIF was used, as it simulates the concentrations of bile acids, phospholipids, and pH in the gastrointestinal lumen [24]. The dissolution rate of rosmarinic acid (RA) in FaSSIF was investigated using RA alone, PM (RA/γ-CD), GM (RA/γ-CD), PM (RA/CD-MOF-1), and GM (RA/CD-MOF-1) samples (Fig. 7B). After 5 min, the dissolution rate of RA alone was approximately 70%, whereas that of PM (RA/γ-CD) was approximately 82%. The dissolution rate of GM (RA/γ-CD) reached approximately 90%, which was higher than that of RA alone and PM (RA/γ-CD). In contrast, PM (RA/CD-MOF-1) and GM (RA/CD-MOF-1) exhibited a dissolution rate of approximately 98%, showing similar performances.

When the CoQ10/γ-CD inclusion complex was dissolved in a NaTC solution, CoQ10 was released from the complex and subsequently micellized with NaTC [47]. Given that the FaSSIF solution used in this study contained NaTC and lecithin, it is plausible that after dissolving GM (RA/CD-MOF-1) in FaSSIF, the released RA was encapsulated in NaTC or NaTC/lecithin rather than in CD-MOF-1. However, because PM (RA/CD-MOF-1) exhibited a dissolution behavior similar to that of GM (RA/CD-MOF-1), it is also possible that the presence of CD-MOF-1 influenced RA solubility through the potassium content of CD-MOF-1. Additionally, encapsulation of RA by NaTC or NaTC/lecithin may

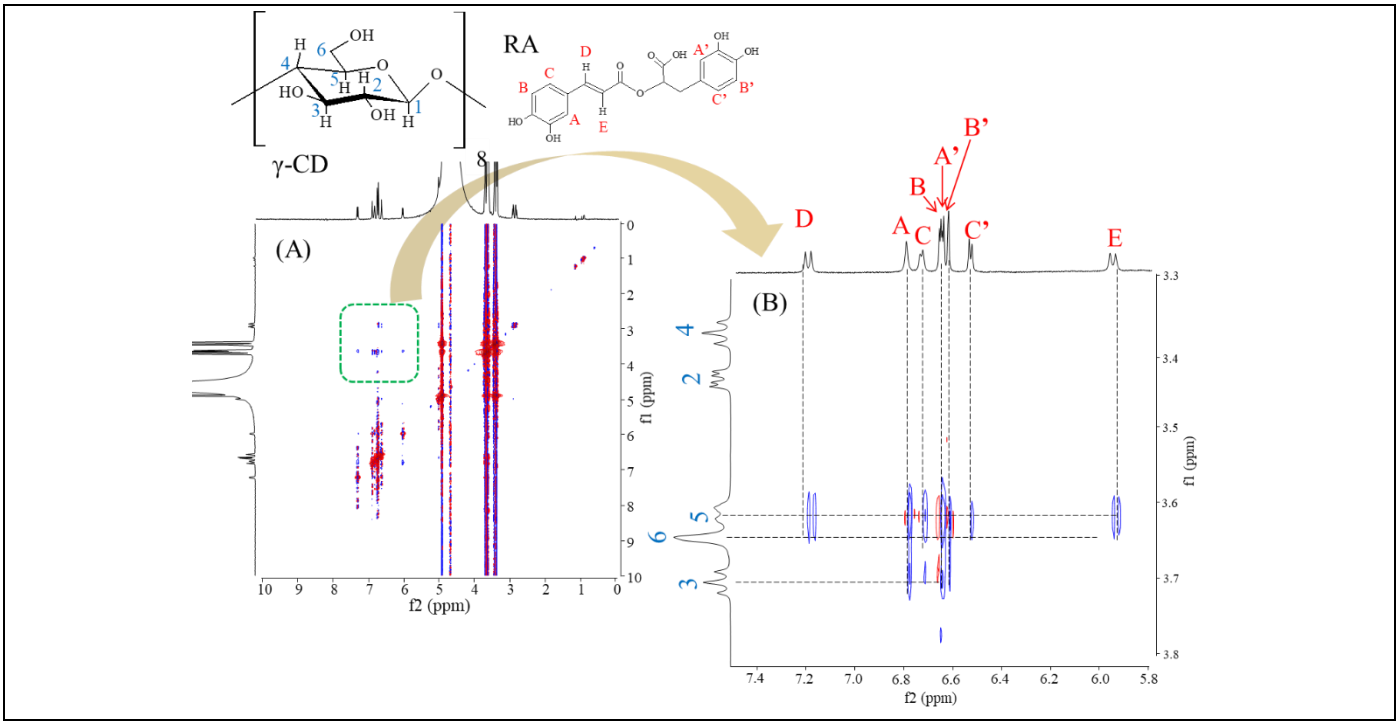

Figure 8A. ^{1}H-^{1}H NOESY NMR spectra of GM (RA/γ-CD) systems. (A) f1 is 0–10 ppm, f2 is 0–10 ppm, (B) f1 is 3.3–3.8 ppm, f2 is 5.8–7.5 ppm

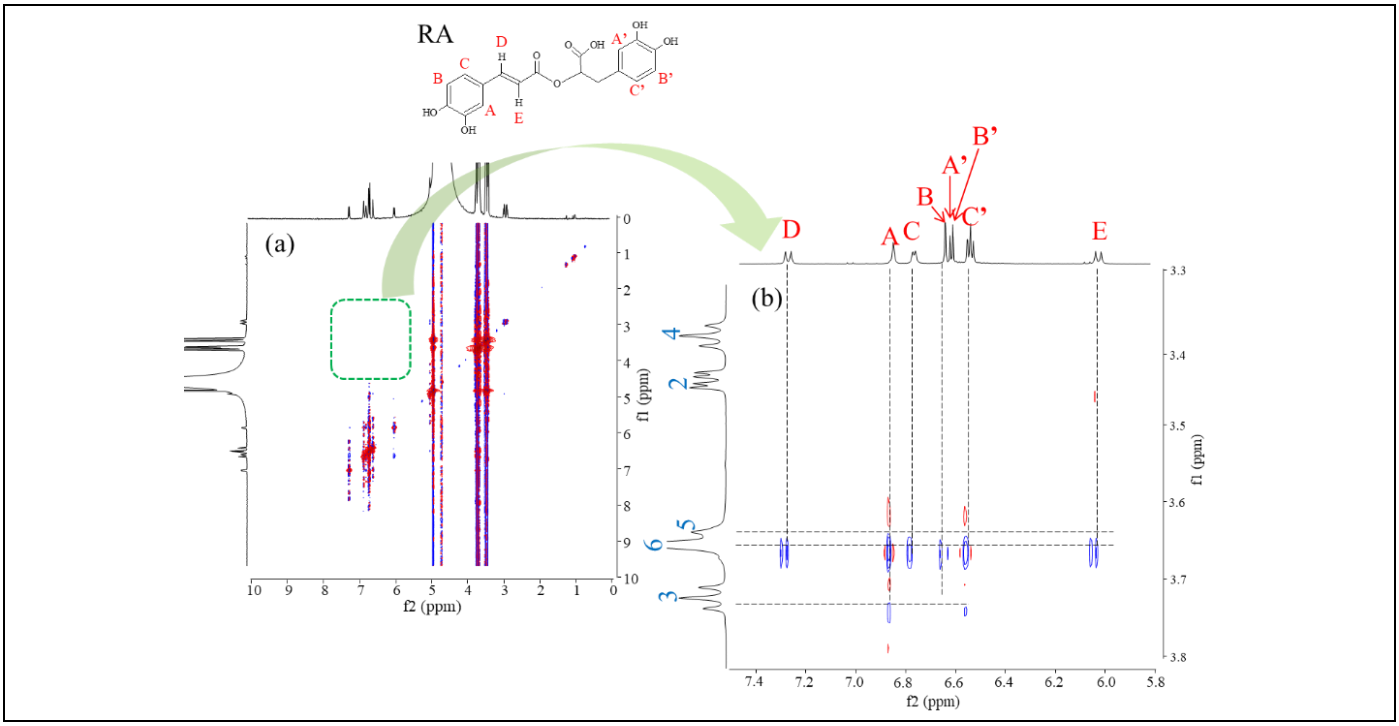

Figure 8B. ^{1}H-^{1}H NOESY NMR spectra of GM (RA/CD-MOF-1) systems. (A) f1 is 0–10 ppm, f2 is 0–10 ppm, (B) f1 is 3.3–3.8 ppm, f2 is 5.8–7.5 ppm

have contributed to its dissolution. Overall, our findings confirm that the formation of an inclusion complex via co-grinding contributed to improved RA solubility. Potassium ligands derived from CD-MOF-1 may also play a role in the dissolution behavior. Although the pH of CD-MOF-1 was not directly measured in this study, its preparation using KOH suggests that it may exhibit mildly alkaline properties, which could influence the dissolution of acidic compounds such as RA.

3.7. ^{1}H-^{1}H NOESY NMR spectroscopy

Although PXRD and DSC patterns alone do not definitively distinguish between amorphous dispersions and inclusion complexes, previous studies, e.g., Aigner et al. Zhao et al. report that halo patterns in PXRD and disappearance of melting peaks in DSC are consistent with inclusion formation [38,39]. In this study, such evidence was further supported by ^{1}H-^{1}H NOESY NMR data showing cross-peaks between RA and the CD cavity protons. To investigate the detailed intermolecular interactions of GM (RA/γ-CD) and GM (RA/CD-MOF-1) in solution, {^{1}H-^{1}H} NOESY NMR measurements were performed. The {^{1}H-^{1}H} NOESY NMR technique is commonly used to confirm interactions between guest molecules and the CD cavity, enabling estimation of the relative position of the inclusion complex [48]. The peak assignments for RA were obtained from a study by Aksamija et al. [49]. The H-3 protons are typically located at the wider rim of the CD ring, whereas the H-6 protons reside at the narrower rim [50]. In GM (RA/γ-CD), cross-peaks were observed between the protons derived from RA, including H-A (6.9 ppm), H-B (6.6 ppm), H-C (6.8 ppm), H-D (7.3 ppm), and H-E (6.0 ppm), as well as H-A′, H-B′ (6.6 ppm), and H-C′ (6.5 ppm), and H-6 protons (3.6 ppm) originating from the inner cavity of the narrower rim of γ-CD. Additionally, cross-peaks were detected between these RA protons and the H-3 protons (3.7 ppm) from the inner cavity of the wider rim of γ-CD (Fig. 8(A)). In contrast, in GM (RA/CD-MOF-1), cross-peaks were observed between the H-6 protons (3.65 ppm) of CD-MOF-1, located at the narrower rim, and the RA-derived protons H-A (6.9 ppm), H-B (6.6 ppm), H-C (6.8 ppm), H-D (7.3 ppm), H-E (6.0 ppm), H-A′, H-B′ (6.6 ppm), and H-C′ (6.5 ppm) (Fig. 7(B)). Moreover, a cross peak was detected between the H-3 proton (3.7 ppm) from the wider rim of the inner cavity of CD-MOF-1 and the H-A proton (6.9 ppm) from RA. These observations indicate that, in GM (RA/CD-MOF-1 = 1/1), the dihydroxyphenyl moiety of RA enters the CD-MOF-1 cavity from the wider rim and extends toward the narrower rim, with the side opposite the vinylene group penetrating first. These results suggest that RA adopts different inclusion modes in GM (RA/CD-MOF-1=1/1) and GM (RA/γ-CD = 1/1). This difference in the inclusion mode may be one of the factors influencing the release behavior of RA.

3.8. DPPH radical-scavenging assay

RA has been reported to exhibit antioxidant activity [51]. Therefore, the antioxidant properties of the inclusion complexes RA/γ-CD and RA/CD-MOF-1

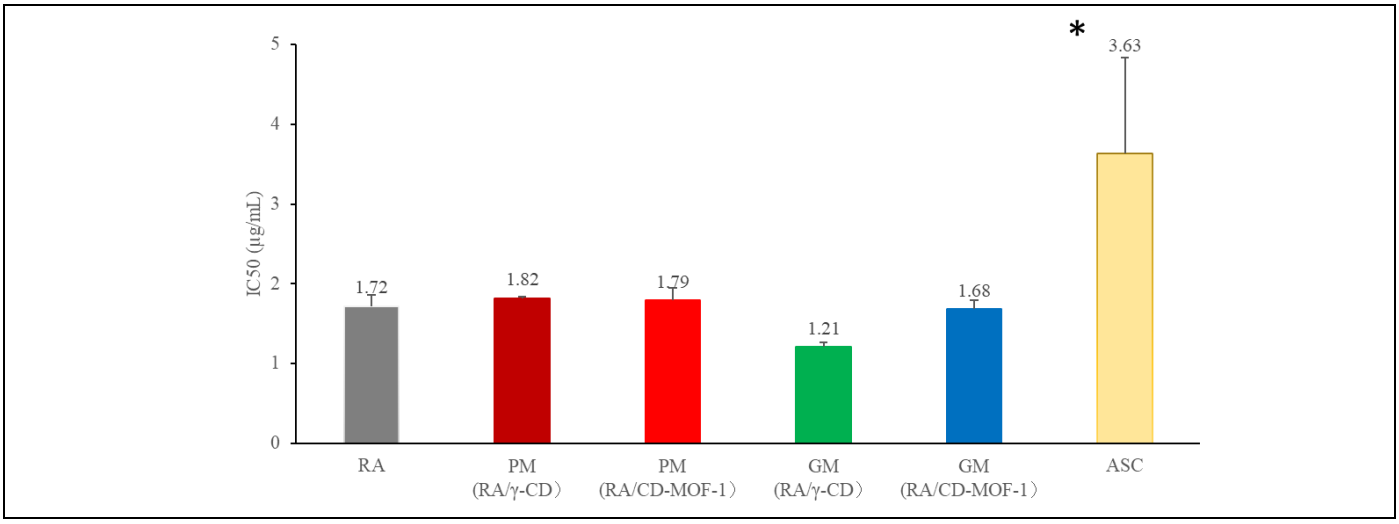

Figure 9 IC_{50} of RA/γ-CD and RA/CD-MOF-1 systems in a DPPH radical scavenging test. Results are expressed as mean ± SD (n = 3). Significant differences were observed for RA (RA-containing samples) compared to a ASC as control, P< 0.05). No significant difference (Tukey's test) between samples containing RA.

were evaluated using a DPPH radical-scavenging assay (Fig. 9). The half-maximal inhibitory concentration (IC_{50}) of intact RA was 1.72 μg/mL (Fig. 9). The IC_{50} values of PM (RA/γ-CD = 1/1) and PM (RA/CD-MOF- was not significant. The IC_{50} of GM (RA/CD-MOF-1 = 1/1) was 1.68 μg/mL. As a reference, the IC_{50} of ascorbic acid, used as a control antioxidant, was 3.63 μg/mL. The reason for this difference in antioxidant effects is that many antioxidants (including RA) are highly lipophilic and have low water solubility; therefore, their antioxidant activities have not been completely clarified. The inclusion of CD, however, may increase their DPPH radical-scavenging capacity by improving their water solubility and increasing their effective concentration in the test system. Inclusion complexes of rosmarinic acid with modified β-cyclodextrins have been reported to markedly enhance its antioxidant activity, along with improvements in solubility and physicochemical stability [30]. In addition, phenolic antioxidants, such as RA, are easily degraded by light, heat, and oxygen, which may reduce their antioxidant capacity. However, the inclusion of CDs may protect them from these external factors and inhibit their degradation, thereby maintaining their antioxidant effect and improving their ability to scavenge DPPH radicals [52,53]. Nevertheless, the inclusion of CDs may properly expose the active antioxidant sites (phenolic hydroxyl groups) of RAs and increase their reactivity with DPPH radicals. Notably, the suitable orientation of RA in the CD cavity may lead to increased contact with DPPH radicals, thus enhancing the reaction kinetics.

4. CONCLUSIONS

PXRD and DSC analyses confirmed the disappearance of the crystalline diffraction peaks and endothermic melting peaks, indicating the successful formation of amorphous inclusion complexes. Dissolution tests showed that RA solubility increased from approximately 70% (RA alone) to 85% (RA/γ-CD) and 95% (RA/CD-MOF-1), demonstrating improved dissolution properties. NOESY NMR spectroscopy revealed specific cross-peaks between RA protons and γ-CD or CD-MOF-1 cavity protons, confirming RA encapsulation within the host structures. The antioxidant capacity of RA was slightly enhanced in the inclusion complexes, suggesting that the CD-MOF-based formulations can improve drug bioavailability and therapeutic efficacy. Although the antioxidant improvements were modest, the findings highlight the potential of CD-MOF-1 as a stabilizing carrier for polyphenolic compounds such as RA. This may contribute to future formulation strategies aimed at improving the solubility, stability, and bioefficacy of phenolic bioactives in pharmaceutical and nutraceutical applications.

5. ACKNOWLEDGEMENTS

The authors wish to thank the Instrument Analysis Center of Josai University for helpful advice on NMR spectrometry. The authors acknowledge the Laboratory of Nutri-Pharmacotherapeutics Management, Josai University, for providing research support while implementing measures against COVID-19 (SARS-CoV-2) infection.

Abbreviation

DPPH	2,2-Diphenyl-1-picrylhydrazyl
DSC	Differential Scanning Calorimetry

GM	Ground Mixture
PM	Physical Mixture
IR	Infrared Spectroscopy
MOF	Metal–Organic Framework
NMR	Nuclear Magnetic Resonance
NIR	Near-Infrared Spectroscopy
NOESY	Nuclear Overhauser Effect Spectroscopy
PXRD	Powder X-ray Diffraction
RA	Rosmarinic Acid
SEM	Scanning Electron Microscopy
IC_{50}	half-maximal inhibitory concentration

Author contribution

Akiteru Ohtsu: Conceptualization, methodology, software, validation, formal analysis, investigation, resources, data curation, writing—original draft preparation, writing—review and editing, visualization, supervision, project administration.

Mione Uchimura: Conceptualization, methodology, software, validation, formal analysis, investigation, resources, data curation, writing—original draft preparation, writing—review and editing, visualization, supervision, project administration.

Nao Kodama: writing—original draft preparation, writing—review and editing, project administration.

Shun-ichi Mitomo: Conceptualization, validation, formal analysis, investigation, writing—original draft preparation, writing—review and editing, project administration.

Junki Tomita: Conceptualization, software, validation, formal analysis, investigation,writing—original draft preparation, writing—review and editing, project administration.

Mitsuaki Suzuki: Conceptualization, validation, formal analysis, investigation,writing—original draft preparation, writing—review and editing, project administration.

Yutaka Inoue: Conceptualization, methodology, software, validation, formal analysis, investigation, resources, data curation, writing—original draft preparation, writing—review and editing, visualization, supervision, project administration, funding acquisition.

Funding

None to declare.

Conflict of interest

None to declare

Ethics approval

None to declare

Article info:

Received May 20, 2025

Received in revised form July 07, 2025

Accepted July 11, 2025

REFERENCES

1. Petersen M, Simmonds MSJ. Rosmarinic acid. Phytochemistry. 2003;62(2):121–125. doi: 10.1016/s0031-9422(02)00513-7.
2. Hitl M, Brkić S, Kladar N. In vitro fermentation of rosmarinic acid and lemon balm (Melissa officinalis L., Lamiaceae) extract by probiotic microorganisms. S Afr J Bot. 2023;157:251–257. doi: 10.1016/j.sajb.2023.04.007.
3. Murugesan R, Vasuki K, Ramadevi S, et al. Rosmarinic acid: potential antiviral agent against dengue virus – in silico evaluation. Intell Pharm. 2024;2(4):528–539. doi: 10.1016/j.ipha.2023.12.006.
4. Veras KS, Fachel FNS, Teixeira HF, et al. Technological strategies applied for rosmarinic acid delivery through different routes – a review. J Drug Deliv Sci Technol. 2022;68:103054. doi: 10.1016/j.jddst.2021.103054.
5. Amoah SKS, Sandjo LP, Kratz JM, et al. Rosmarinic acid—pharmaceutical and clinical aspects. Planta Med. 2016;82(5):388–406. doi: 10.1055/s-0035-1568274.
6. Kim HK, Hwang S, Sung B, et al. Gd-complex of a rosmarinic acid conjugate as an anti-inflammatory theranostic agent via reactive oxygen species scavenging. Antioxidants (Basel). 2020;9(8):744. doi: 10.3390/antiox9080744.
7. Erkan N, Ayranci G, Ayranci E. Antioxidant activities of rosemary (Rosmarinus officinalis L.) extract, blackseed (Nigella sativa L.) essential oil, carnosic acid, rosmarinic acid and sesamol. Food Chem. 2008;110(1):76–82. doi: 10.1016/j.foodchem.2008.01.058.
8. Noor S, Mohammad T, Rub MA, et al. Biomedical features and therapeutic potential of rosmarinic acid. Arch Pharm Res. 2022;45(4):205–228. doi: 10.1007/s12272-022-01378-2.
9. Azhar MK, Anwar S, Hasan GM, et al. Comprehensive insights into biological roles of rosmarinic acid: implications in diabetes, cancer and neurodegenerative diseases. Nutrients. 2023;15(19):4297. doi: 10.3390/nu15194297.
10. Usha T, Middha SK, Bhattacharya M, et al. Rosmarinic acid, a new polyphenol from Baccaurea ramiflora Lour. leaf: a probable compound for its anti-inflammatory activity. Antioxidants (Basel). 2014;3(4):830–842. doi: 10.3390/antiox3040830.
11. Wang J, Li G, Rui T, et al. Pharmacokinetics of rosmarinic acid in rats by LC-MS/MS: absolute bioavailability and dose proportionality. RSC Adv. 2017;7(15):9057–9063. doi: 10.1039/C6RA28237G.
12. Fateminasab F, Bordbar AK, Asadi B, et al. Modified β-cyclodextrins: rosmarinic acid inclusion complexes as functional food ingredients show improved operations (solubility, stability and antioxidant activity). Food Hydrocoll. 2022;131:107731. doi: 10.1016/j.foodhyd.2022.107731.
13. Mason JA, Veenstra M, Long JR. Evaluating metal–organic frameworks for natural gas storage. Chem Sci. 2014;5(1):32–51. doi: 10.1039/C3SC52633J.
14. Ma S, Zhou HC. Gas storage in porous metal–organic frameworks for clean energy applications. Chem Commun (Camb). 2010;46(1):44–53. doi: 10.1039/b916295j.
15. Li B, Wen HM, Zhou WB, et al. Porous metal–organic frameworks for gas storage and separation: what, how, and why? J Phys Chem Lett. 2014;5(20):3468–3479. doi: 10.1021/jz501586e.
16. Lopez ECR, Perez JVD. CD-MOFs for CO_2 capture and separation: current research and future outlook. Eng Proc. 2023;56(1):65. doi: 10.3390/ASEC2023-15374.
17. Li JR, Sculley J, Zhou HC. Metal–organic frameworks for separations. Chem Rev. 2012;112(2):869–932. doi: 10.1021/cr200190s.
18. Horcajada P, Gref R, Baati T, et al. Metal–organic frameworks in biomedicine. Chem Rev. 2012;112(2):1232–1268. doi: 10.1021/cr200256v.

19. Smaldone RA, Forgan RS, Furukawa H, et al. Metal–organic frameworks from edible natural products. Angew Chem Int Ed Engl. 2010;49(46):8630–8634. doi: 10.1002/anie.201002343.
20. Bello MS, Kumar R, Singh P, et al. Cyclodextrin metal–organic framework design principles and functionalization for biomedical application. Carbohydr Polym. 2025;317:121029. doi:10.1016/j.carbpol.2025.121029.
21. Patyk-Kaźmierczak E, Warren MR, Allan DR, et al. Pressure inverse solubility and polymorphism of an edible γ-cyclodextrin-based metal–organic framework. Phys Chem Chem Phys. 2017;19(13):9086–9091. doi: 10.1039/C7CP00593H.
22. Hartlieb KJ, Holcroft JM, Moghadam PZ, et al. CD-MOF: a versatile separation medium. J Am Chem Soc. 2016;138(7):2292–2301. doi: 10.1021/jacs.5b12860.
23. Nanri A, Yoshida M, Ishida Y, et al. Preparation and characterization of a hybrid complex of cyclodextrin-based metal–organic frameworks-1 and ascorbic acid derivatives. Materials (Basel). 2021;14(23):7309. doi: 10.3390/ma14237309.
24. Inoue Y, Yoshida M, Ezawa T, et al. Inclusion complexes of daidzein with cyclodextrin-based metal-organic framework-1 enhance its solubility and antioxidant capacity. AAPS PharmSciTech. 2021;23(1):2. doi: 10.1208/s12249-021-02151-2.
25. Liu J, Bao TY, Yang XY, et al. Controllable porosity conversion of metal–organic frameworks composed of natural ingredients for drug delivery. Chem Commun (Camb). 2017;53(55):7804–7807. doi: 10.1039/C7CC03673F.
26. Anselmi C, Centini M, Ricci M, et al. Analytical characterization of a ferulic acid/γ-cyclodextrin inclusion complex. J Pharm Biomed Anal. 2006;40(4):875–881. doi: 10.1016/j.jpba.2005.08.019.
27. Zoppi A, Delrivo A, Aiassa V, et al. Binding of sulfamethazine to β-cyclodextrin and methyl-β-cyclodextrin. AAPS PharmSciTech. 2013;14(2):727–735. doi: 10.1208/s12249-013-9958-9.
28. Aigner Z, Berkesi O, Farkas G, et al. DSC, X-ray and FTIR studies of a gemfibrozil/dimethyl-β-cyclodextrin inclusion complex produced by co-grinding. J Pharm Biomed Anal. 2012;57:62–67. doi: 10.1016/j.jpba.2011.08.034.
29. Esteso MA, Romero CM. Cyclodextrins: properties and applications. Int J Mol Sci. 2024;25(8):4547. doi: 10.3390/ijms25084547.
30. Oves M, Khan MS, Zaidi A, et al. Modified β-cyclodextrins: Rosmarinic acid inclusion complexes as functional food ingredients show improved operations (solubility, stability and antioxidant activity). Food Hydrocoll. 2023;131:107731. doi:10.1016/j.foodhyd.2022.107731.
31. Kleyton R, Silva V, Souza A, et al. Cyclodextrin derivatives as promising solubilizers to enhance the biological activity of rosmarinic acid. J Drug Deliv Sci Technol. 2023;81:104312. doi:10.1016/j.jddst.2022.104312.
32. Ohashi H, Yamada K, Fujii K, et al. Application of cyclodextrin-based metal–organic frameworks for multi-drug carriers: A combined experimental and simulation study. Int J Pharm. 2025;634:123456. doi:10.1016/j.ijpharm.2025.123456.
33. Zhao Y, Li W, Zhang M, et al. Metal–organic frameworks (MOFs) and their derivatives as emerging biomaterials in biomedicine. Front Pharmacol. 2024;15:1462368. doi:10.3389/fphar.2024.1462368.
34. Ikeda N, Inoue Y, Ogata Y, Murata I, Xuan M, Takayama J, et al. Improvement of the solubility and evaluation of the physical properties of an inclusion complex formed by a new ferulic acid derivative and γ cyclodextrin. ACS Omega. 2020;5(21):12073 12080. doi:10.1021/acsomega.0c00277.
35. Vertzoni M, Fotaki N, Kostewicz E, et al. Dissolution media simulating the intralumenal composition of the small intestine: physiological issues and practical aspects. J Pharm Pharmacol. 2004;56(4):453–462. doi: 10.1211/0022357022935.
36. Chao J, Wang H, Zhao W, et al. Investigation of the inclusion behavior of chlorogenic acid with hydroxypropyl-β-cyclodextrin. Int J Biol Macromol. 2012;50(1):277–282. doi: 10.1016/j.ijbiomac.2011.11.008.
37. Meng F, Wang J, He J, et al. Inclusion complex of baicalin with hydroxypropyl-β-cyclodextrin: preparation, characterization and in vitro dissolution studies. Molecules. 2012;17(6):5976–5987. doi: 10.3390/molecules17065976.
38. Zhao Y, Ren J, Wang Y, et al. Preparation, characterization and antioxidant activity of inclusion complex of luteolin with hydroxypropyl-β-cyclodextrin. J Food Sci Technol. 2015;52(8):5055–5061. doi: 10.1007/s13197-014-1606-7.
39. Duchêne D, Bochot A. Thirty years with cyclodextrins. Int J Pharm. 2016;514(1):58–72. doi: 10.1016/j.ijpharm.2016.06.044.
40. Loftsson T, Duchêne D. Cyclodextrins and their pharmaceutical applications. Int J Pharm. 2007;329(1–2):1–11. doi: 10.1016/j.ijpharm.2006.10.044.
41. Hedges AR. Industrial applications of cyclodextrins. Chem Rev. 1998;98(5):2035–2044. doi: 10.1021/cr970010b.
42. Szente L, Szejtli J. Highly soluble cyclodextrin derivatives: chemistry, properties, and trends in development. Adv Drug Deliv Rev. 2004;56(8):1821–1830. doi: 10.1016/j.addr.2004.02.017.
43. Lavasanifar A, Samuel J, Kwon GS. Poly(ethylene oxide)-block-poly(L-amino acid) micelles for drug delivery. Adv Drug Deliv Rev. 2002;54(2):169–190. doi: 10.1016/S0169-409X(02)00017-5.
44. Szente L, Singhal A, Domokos A, Song BW. Cyclodextrins: Assessing the impact of cavity size, occupancy, and substitutions on cytotoxicity and cholesterol homeostasis. Molecules. 2018;23(5):1228. doi: 10.3390/molecules23051228.
45. Cserháti T, Forgács E, Oros G. Biological activity and environmental impact of anionic surfactants. Environ Int. 2002;28(5):337–348. doi: 10.1016/S0160-4120(02)00042-6.
46. Szente L, Fenyvesi É. Cyclodextrin–lipid complexes: cavity size matters. Struct Chem. 2017;28(5):1305–1313. doi: 10.1007/s11224-017-0976-3.
47. Uekaji Y, Jo A, Ohnishi M, et al. A new generation of nutra-ceuticals and cosme-ceuticals complexing lipophilic bioactives with γ-cyclodextrin. Procedia Eng. 2012;36:540–550. doi: 10.1016/j.proeng.2012.03.079.
48. Shiozawa R, Inoue Y, Murata I, et al. Effect of antioxidant activity of caffeic acid with cyclodextrins using ground mixture method. Asian J Pharm Sci. 2018;13(1):24–33. doi: 10.1016/j.ajps.2017.08.006.
49. Aksamija A, Polidori A, Plasson R, et al. The inclusion complex of rosmarinic acid into beta-cyclodextrin: a thermodynamic and structural analysis by NMR and capillary electrophoresis. Food Chem. 2016;208:258–263. doi: 10.1016/j.foodchem.2016.04.008.
50. Lis-Cieplak A, Sitkowski J, Kolodziejski W. Comparative proton nuclear magnetic resonance studies of amantadine complexes formed in aqueous solutions with three major cyclodextrins. J Pharm Sci. 2014;103(1):274–282. doi: 10.1002/jps.23802.
51. Baba S, Osakabe N, Natsume M, et al. Absorption and urinary excretion of rosmarinic acid after intake of Perilla frutescens extract in humans. Eur J Clin Nutr. 2005;59(4):1–9. doi: 10.1007/s00394-004-0482-2.
52. Żyżelewicz D, Oracz J, Kaczmarska M, et al. Preparation and characterization of inclusion complex of (+)-catechin with β-cyclodextrin. Food Res Int. 2018;113:263–268. doi: 10.1016/j.foodres.2018.07.018.
53. Shin GH, Kim JT, Park HJ. Recent developments in nanoformulations of lipophilic functional foods. Trends Food Sci Technol. 2015;46(1):144–157. doi: 10.1016/j.tifs.2015.07.005.